Z. Phys. A Manuscript-Nr.
(will be inserted by hand later)

K^+-meson production in pBe interactions at T_p = 2.9 GeV

M. Büscher[1], R. Eßer[1], A. Franzen[1], L.v. Horn[1], D. Kopyto[1], H. Ohm[1], H. Seyfarth[1], K. Sistemich[1], H. Müller[2], B. Prietzschk[2], B. Rimarzig[2], C. Schneider[2], C. Schneidereit[2], A. Akindinov[3], M. Chumakov[3], V. Demechin[3], V. Ergakov[3], A. Gerasimov[3], V. Goryachev[3], Y. Kiselev[3], V. Kostromin[3], A.A. Sibirtsev[3,4], V. Sopov[3], V. Tchernyshev[3], V. Kruglov[4], A. Petrus[4], V. Koptev[5], and S. Mikirtychyants[5]

[1] Institut für Kernphysik, Forschungszentrum Jülich, Postfach 1913, D-52425 Jülich, Germany
[2] Institut für Kern- und Hadronenphysik, Forschungszentrum Rossendorf, Postfach 510119, D-01314 Dresden, Germany*
[3] Institute of Theoretical and Experimental Physics, Cheremushkinskaya 25, 117259 Moscow, Russia
[4] Laboratory of Nuclear Problems, Joint Institute of Nuclear Research, 141980 Dubna, Russia**
[5] High Energy Physics Department, Petersburg Nuclear Physics Institute, 188350 Gatchina, Russia

Received:

Abstract. The production of K^+ and π^+ mesons and protons in pBe collisions at T_p = 2.9 GeV has been studied at the ITEP proton synchrotron. Ejectiles with a momentum of p = 545 MeV/c were observed under an emission angle $\vartheta = 17°$. The detectors which have been developed for the identification of kaons out of a six orders of magnitude more intense background of pions and protons are described. A cross-section ratio $\mathrm{d}^2\sigma_{K^+}/\mathrm{d}\Omega\mathrm{d}p$: $\mathrm{d}^2\sigma_{\pi^+}/\mathrm{d}\Omega\mathrm{d}p$: $\mathrm{d}^2\sigma_p/\mathrm{d}\Omega\mathrm{d}p$ of (1 ± 0.34):(85 ± 1):(31 ± 1) has been measured. Normalization with existing pion data yields an invariant differential cross section $E \cdot \mathrm{d}^3\sigma_{K^+}/\mathrm{d}^3p = (3.1 \pm 1.2)$ mb GeV^{-2} c^3 sr^{-1} and a total cross section of $\sigma_{\mathrm{tot}}(p\mathrm{Be}) = (3.7 \pm 1.5)$ mb. These cross sections are compared with existing data and theoretical predictions. The A dependence of K^+ production in the few-GeV range is analyzed.

PACS: 25.40.−h; 13.75.−n

1 Introduction

The production of K^+ mesons in proton-nucleus collisions has attracted considerable interest both from the experimental as from the theoretical side. Due to strangeness conservation K^+ mesons only weakly interact with the surrounding nuclear medium and, therefore, can carry out of the nucleus with minimal distortions the information about the production mechanism. This is why their observation may indicate whether they have been created in a quark-gluon plasma or in a hadronic phase. It was pointed out [1, 2] that the spectra of K^+ mesons may be sensitive to the different production mechanisms and the nuclear spectral function.

In the present study we have measured K^+, π^+ and p production in pBe collisions at an incident energy of T_p = 2.9 GeV. The ejectiles were detected under emission angles of $\vartheta = 17°$ and momenta p = 545 MeV/c. This kinematical region is of special interest since it was predicted [1, 2] that at $T_p > 2$ GeV and at forward production angles the kaons are produced in the interaction of the incident proton with a single target nucleon i.e. in the direct reaction mechanism $pN \to K^+X$. On the other hand, contributions from secondary processes ($pN_1 \to \pi X, \pi N_2 \to K^+Y$) are expected to be negligible. In order to achieve most clear conditions we have chosen a light target (Be) where the pion-rescattering probability is small and, thus, contaminations from secondary processes are even more suppressed. From the measured cross-section ratios we extract the total K^+-production cross section for pBe collisions and compare it with existing data as well as with theoretical predictions.

For the measurements a detection system was used which is a prototype of telescopes prepared for subthreshold K^+ studies [1, 2] at small cross sections with the 0° Facility `ANKE' at COSY Jülich [3, 4]. We show that these detectors offer a high kaon-detection efficiency of 34% and simultanously a pion and proton suppression by more than six orders of magnitude. The measured performance of the system is in good agreement with results from simulation calculations.

2 Experimental setup

The measurements were carried out at the ITEP (Institute of Theoretical and Experimental Physics, Moscow) synchrotron where proton beams with energies of $T_p \leq 10$ GeV and intensities up to 3×10^{11} particles per bunch are available. For our experiment a thin ($d \approx 0.2$ mm) internal Be target was chosen. Secondary particles produced under $\vartheta = 17°$ were analyzed using the N530 beam channel [5]. It consists of two bending dipoles (D1, D2) and six quadrupole magnets (Q1–Q6) for momentum analysis in the range $0.4 < p < 1.4$ GeV/c, see Fig. 1. Furthermore, two electrostatic elements (S1, S2) allow to separate particles with equal momentum but different masses and, thus, kaon, pion and proton beams with less than 1% admixture of other particles are available. These pure particle beams have been used to determine the detection efficiencies of our counters for kaons, pions and protons. With the electrostatic separators S1 and S2 switched off one obtains a mixed beam with equal geometrical acceptances for kaons, pions and protons. Thus, one can extract the cross-section ratio $\sigma(K^+)$:$\sigma(\pi^+)$:$\sigma(p)$ from a measurement of

* Supported by the Bundesministerium für Forschung und Technologie, Germany
** Supported by RFFR grant 93-02-3795

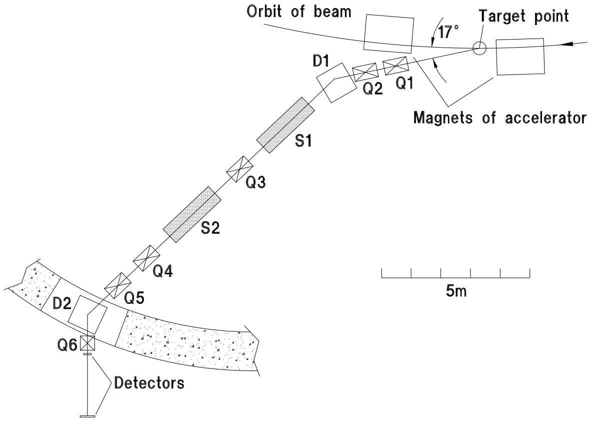

Fig. 1. Sketch of the N530 beam channel at ITEP

the particle rates behind the separator taking into account the detection efficiencies for the different particles obtained from the separated beams and correcting for particle-decay in flight. The momentum and angular acceptance of the separator are $\Delta p/p \approx 2\%$ and $\Delta\Omega \approx 0.6$ msr, respectively; the total length of the flight path between the target and the TOF-stop counter was 21.9 m. Kaons, pions and protons were detected with a telescope consisting of a TOF system as well as Cerenkov, ΔE and veto counters.

Due to their mass difference kaons, pions and protons of equal momenta have different velocities and, thus, can be distinguished with the help of TOF and Cerenkov counters. For the TOF measurement a start counter from Pilot U – 2 mm thick, 5 cm wide and 30 cm long – was placed vertically close to the exit window of the beam line. Each end of the scintillator was coupled to a 30 cm long twisted Plexiglas light guide which led to a photomultiplier (PM) tube Philips XP 2972. Additionally, a second scintillator strip – 4 mm thick, 3 cm wide and 30 cm long – was oriented perpendicular to the first scintillator in order to serve as an active collimator which accepts only those particles which passed through the overlap region of both scintillators ($3 \times 5\text{cm}^2$). This scintillator was read out with PM tubes XP 2020. The use of the two crossed start counters assures that only particles within a well defined area are accepted and minimizes background from accidential coincidences and particles scattered in the beam channel.

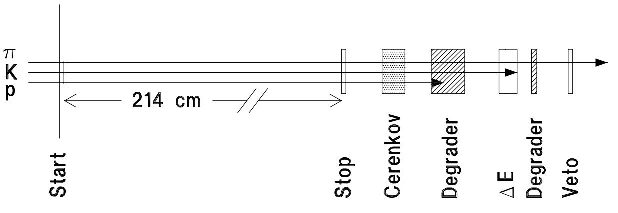

Fig. 2. Sketch of the telescope which was used for the measurements at ITEP

The TOF-stop counter was placed 214 cm downstream of the horizontal start counter in front of the remaining components of the telescope, see Fig. 2 and Table 1. All these detectors had the same width (10 cm) and height (100 cm) and were mounted in a vertical position. Each end of the scintillator strips was glued to a fish-tail light guide which was then coupled to a PM tube XP 2020.

For the Cerenkov counter also XP 2020 PM tubes were used, however without light guides. For our measurements we employed a threshold-Cerenkov counter with an index of refraction $n = 1.49$. This corresponds to minimum momenta for the emission of Cerenkov light of $p_{\text{min}} = 450$ MeV/c (127 MeV/c, 854 MeV/c) for the kaons (pions, protons). Since the kaon momentum was only slightly above the Cerenkov threshold, the amount of produced Cerenkov light is small. Furthermore, most of the light is emitted under small angles relative to the kaon trajectories and cannot reach the PM tube via total reflection. Therefore, in our measurement the kaons (and protons) were identified as those particles which produce no or only small signals in the Cerenkov counter (see also Chap. 3).

In principle, the different energy losses $\mathrm{d}E/\mathrm{d}x$ of kaons, pions and protons with equal momenta can be used to distinguish between these particles. However, for the momenta in our measurement the difference is small, in particular for kaons and pions ($\mathrm{d}E/\mathrm{d}x(K^+) : \mathrm{d}E/\mathrm{d}x(\pi^+) \approx 1.3$). Thus, we used a degrader in front of the ΔE counter in order to maximize the ΔE ratio of kaons and pions. This first degrader stopped the protons and slowed down the kaons such that the latter were stopped at the end of the ΔE counter yielding a maximum energy loss for kaons in this counter whereas the pion energy loss was almost unaffected by the degrader and small. Thus, a substantially better separation of kaons and pions in the ΔE spectra can be achieved ($\Delta E(K^+) : \Delta E(\pi^+) \approx 3$), see also Fig. 5 in Chap. 3. The second degrader prevented kaons from entering the veto counter which ideally should only detect the pions. The thicknesses of both degraders provided the tuning to the ejectile momentum of 545 MeV/c. They were optimized during the experiment. The veto counter will later, at the 0° Facility, mainly be used for the rejection of ejectiles scattered in the spectrometer. It turned out that this counter did not improve the performance of the detection system for the measurements described here and, thus, its proporties are not described in Chap.3.

Table 1. Components of the counter telescopes. Also shown are the kinetic energies T of the detected particles in front of each counter calculated with the Bethe-Bloch formula. The values for $T(K^+)$ in front of and behind the ΔE counter should only be regarded as an estimate due to the uncertainties in the Bethe-Bloch formula for large energy losses

Component	material	thickness	T [MeV]		
			π^+	K^+	p
Start counter #1, hor.	Pilot U	0.4 cm	423	242	147
Start counter #2, vert.	Pilot U	0.2 cm	422	241	145
Stop counter	BC 408	1.0 cm	421	240	143
Cerenkov counter	GS 218	5.0 cm	419	237	138
Degrader #1	iron	7.4 cm	409	223	107
ΔE counter	BC 408	4.0 cm	321	66	–
Degrader #2	iron	1.2 cm	314	42	–
Veto counter	BC 408	1.0 cm	303	–	–

The data acquisition was based on a CAMAC system controlled by a PC with the software package CAMDA [6]. For each PM tube amplitudes and arrival times of the signals were measured with LeCroy Fera QDCs and TDCs. The system gate signal was generated by a coincidence between the two start counters and the stop counter. For both start counters and the stop counter corrections for the light propagation time were made using analog meantimers FDMT 101. Arrival times of all signals were measured with respect to the output of the horizontal start-counter meantimer. The counting rate during the measurements was below $2 \cdot 10^4\ \mathrm{s}^{-1}$ leading to negligible distortions through chance coincidences.

3 Data analysis

Figure 3a shows a TOF spectrum for pions and protons measured with the unseparated beam (S1, S2 switched off). It can be seen that there is only little background outside the pion and proton peaks from other particles or ejectiles scattered in the separator. Due to the low production cross section and decay-in-flight no kaons are visible in the spectrum. From the spectra a time resolution (FWHM) of 580 ps for pions and 440 ps for protons has been deduced. The TOF difference of the pions and protons (Δ_{TOF} = 6.8 ns) has been used to analytically determine the momenta of the detected ejectiles. We obtain a value of p = 545 MeV/c. This value is in agreement with the result of simulation calculations using GEANT 3.15 including energy losses in all components of the detection system. These simulations show that the mean ejectile momenta can be determined with an accuracy better than 1%. According to previous measurements [5] the momentum acceptance of the separator is $\sim$ 2%. This number is well reproduced by our simulation calculations which were performed for a momentum spread of 2% and reproduce the shape of all measured spectra. Fig. 3b shows a TOF spectrum measured with a separated K^+ beam (S1, S2 switched on). It can be seen that – as in the case of the pion and proton spectra – there is only very little background outside the kaon peak and, in particular, there are no events stemming from pions or protons visible in the spectrum. The apparent events around the position of the π^+ TOF peak are caused by muons from kaon decay ($K^+ \to \mu^+\nu_\mu$) between the exit of the separator and the TOF-stop counter. This is also confirmed by our simulation calculations.

In order to minimize background from misidentified particles and from ejectiles scattered in the separator only those events lying inside the shaded areas in Fig. 3 were accepted leading to a detection probability of $\sim$ 95% for the K^+ (π^+, p) relative to the number of all events in the corresponding TOF spectra. The efficiencies for all other detectors (A_{stop}, Cerenkov and ΔE, see below) are given as a fraction of the number of these `valid' events. This choice of the TOF gates assures that – in the case of the separated beams – contaminations from other particles can completely be rejected and, thus, an unambigous particle identification via TOF can be achieved. Thus calibration of the other counters is easily possible. It should be mentioned that the numbers on the detection efficiencies and background suppressions given below are – within statistical fluctuations – independent of the width of the gates in the TOF spectra (shaded areas in Fig. 3). Furthermore, previous measurements at ITEP [7] showed that the e^+/π^+ rate ratio is less than 2% and, therefore, contaminations from e^+ do not affect the measured π^+-production cross sections.

Table 2 shows the identification efficiencies for kaons, pions and protons which have been measured in different runs with pure secondary-particle beams. The difference of the mean energy losses of kaons (2.6 MeV), pions (2.0 MeV) and protons (5.5 MeV) in the TOF-stop counter and, thus, the different measured amplitudes in the stop counter (A_{stop}) allows a moderate separation between these particles. Gates were set such that 87% (99%, 96%) of all kaons (pions, protons) are detected, see column `A_{stop}' in Table 2.

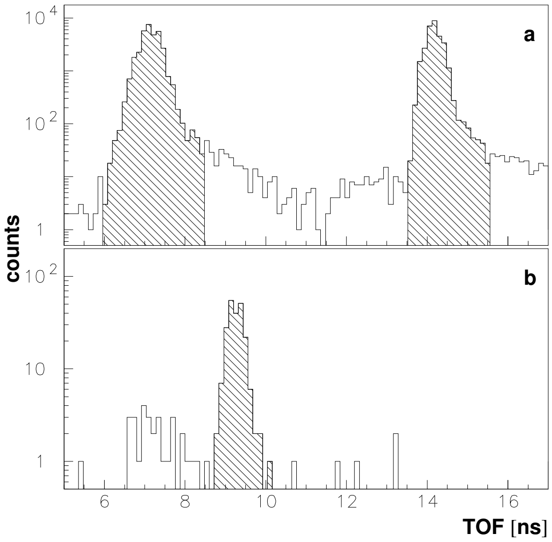

Fig. 3. Measured time-of-flight spectrum of **a** pions, protons and **b** kaons. The positions of the TOF gates which define `valid' pion, proton and kaon events are indicated

Table 2. Identification efficiencies for kaons, pions and protons in the various counters. The efficiencies for the A_{stop}, Cerenkov and ΔE spectra are given relative to the number of events which lie inside the corresponding TOF gate (see text and Fig. 3). The efficiencies deduced from GEANT simulations are given in parentheses

	A_{stop}	C	ΔE	total
K^+	0.87 (0.94)	0.95	0.37 (0.45)	0.34 ± 0.05
π^+	0.99 (0.95)	0.90	0.55 (0.59)	0.55 ± 0.02
p	0.96 (0.99)	0.95	1.00 (1.00)	0.91 ± 0.01

Figure 4 shows the Cerenkov spectra of kaons and pions obtained with separated particle beams and the corresponding gates set for the identification of these particles. As mentioned in Chap. 2 the kaon momentum lies above the threshold for Cerenkov-light emission (p_{min} = 450 MeV/c) but the signal amplitudes in this counter are very small or zero. Thus, with the gate indicated in Fig. 4 95% of all kaons are identified correctly as those events with small Cerenkov amplitudes. For the pions we achieve an identification efficiency of 90%. Although the proton momenta are below the threshold for Cerenkov-light emission (854 MeV/c) 5% of them are misidentified in the Cerenkov counter. This is due to the production of fast particles in proton induced reactions like δ electrons or fast pions from the reaction $pp \to \pi X$.

Since protons were stopped in the first degrader (as indicated in Fig. 2 and Table 1) they do not show up in the ΔE spectra and, thus, protons can be identified as those particles giving no signal in the ΔE counter. The detection probability for kaons in the ΔE counter is only 37% since kaons are scat-

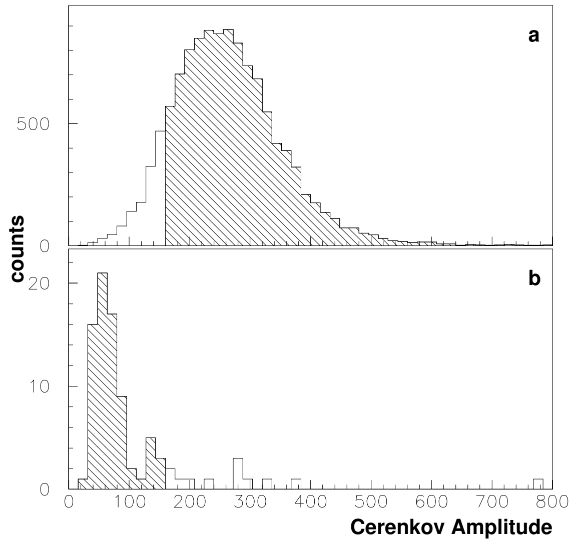

Fig. 4. Cerenkov spectra of **a** pions and **b** kaons. The gates set for the identification of the different particles are indicated

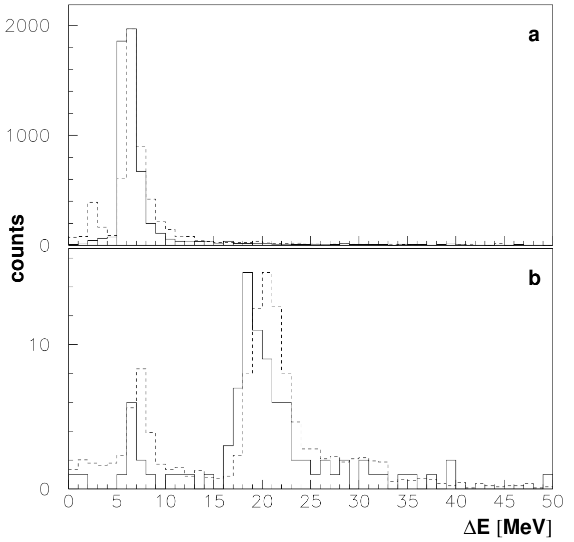

Fig. 5. ΔE spectra of **a** pions and **b** kaons. The measured and simulated spectra are shown as *solid* and *dashed lines*, respectively

tered out of the telescope by the degrader or get lost in hadronic interactions. Figure 5 shows the ΔE spectra of kaons and pions obtained with separated particle beams. The low-energy peak in the kaon spectrum around 7 MeV is caused by decay muons ($K^+ \rightarrow \mu^+\nu_\mu$). Also shown in Fig. 5 are the results of GEANT-simulation calculations. For the simulations GEANT 3.15 modified with MicRes, a code for hadronic interactions in the few-GeV region, was used [8]. There is good agreement of the peak positions and shapes between the measured and simulated spectra.

Column `total' in Table 2 shows the detection efficiency of the telescope if the corresponding gates on all available spectra (TOF, A_{stop}, Cerenkov and ΔE) were set. We achieve an efficiency of $(34\pm5)\%$ ($(55\pm2)\%$, $(91\pm1)\%$) of correctly identified kaons (pions, protons) relative to the number of particles which lie inside the corresponding TOF gates shown in Fig. 3. Note that the total efficiency is not simply the product of the individual efficiencies since here statistically independent quantities were measured.

Table 3 shows the suppression factors for pions and protons if the gates in the various spectra were set for kaon detection. First, the data obtained with the separated K^+ beam were used to determine the position of the gates in the various spectra for kaon detection (see Fig. 3b and 4b). Then the remaining fractions of pions and protons between these kaon gates were determined from the pion and proton data.

Table 3. Fractions of misidentified pions and protons in the various spectra if gates were set for kaon detection. As explained in Chap. 2 the Cerenkov counter cannot discriminate kaons against protons. The results of the GEANT simulations are given in parentheses

	TOF	A_{stop}	C	ΔE	total
π^+	0.0037	0.13(0.13)	0.10	0.035(0.034)	$3 \cdot 10^{-7}$
p	0.0044	0.01(0.001)	1.00	0.0003(0.0005)	$3 \cdot 10^{-7}$

The total background-suppression factors of $3 \cdot 10^{-7}$ for pions and protons which is obtained from a simultanous application of the TOF, A_{stop}, Cerenkov and ΔE information allows the measurement of very low kaon rates in a high background of pions and protons. Thus, our measurements show that the telescope tested here is also well suited for the study of subthreshold K^+ production where the cross sections are extremely small (in the few-nanobarn range). Such studies are planned for the 0° Facility `ANKE' at COSY-Jülich [3, 4].

It should be noted that the measured background-suppression factors using the ΔE informations are in good agreement with the results of simulation calculations which are also shown in Table 3. The background suppression factors of the Cerenkov counter have not been compared with simulation calculations since such counters cannot be modelled within GEANT 3.15. The shape of the TOF spectra is mainly determined by counter characteristics like light propagation in the scintillator and photomultiplier properties and, therefore, background suppression from TOF has not been simulated.

For the measurement of the cross-section ratios $\sim 8 \cdot 10^5$ events were written on tape during $\sim$ 24 hours with unseparated beam. Using the gates obtained with separated beams 11 kaons, $\sim 1.6 \cdot 10^5$ pions and $\sim 2.0 \cdot 10^5$ protons were identified. From the pion and proton suppression factors of $3 \cdot 10^{-7}$ given in Table 3 it can be concluded that the background of pions and protons misidentified as kaons is zero. The numbers for the detected particles were corrected for the identification efficiencies from Table 2 and for particle decay-in-flight (only $\sim 0.5\%$ of all K^+ survive) between the target and the counters yielding a production cross-section ratio of

$$\frac{\mathrm{d}^2\sigma}{\mathrm{d}\Omega\mathrm{d}p}(K^+) \;:\; \frac{\mathrm{d}^2\sigma}{\mathrm{d}\Omega\mathrm{d}p}(\pi^+) \;:\; \frac{\mathrm{d}^2\sigma}{\mathrm{d}\Omega\mathrm{d}p}(p) = (1\pm0.34) : (85\pm1) : (31\pm1)\,. \tag{1}$$

All quoted errors are of statistical nature.

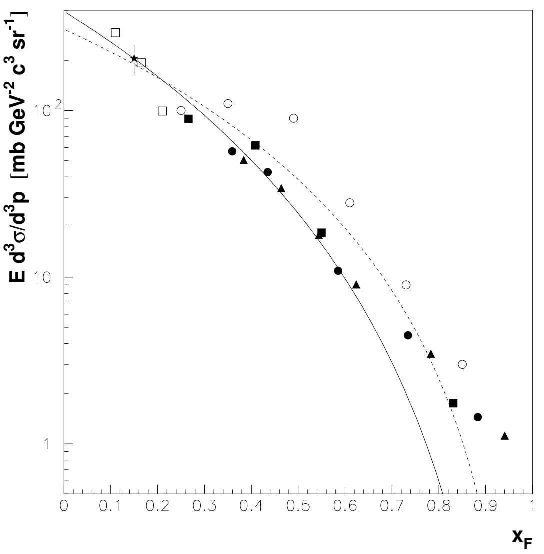

Fig. 6. Measured invariant cross sections for π^+ production. Closed symbols show the pion spectra measured at an emission angle of 3.5° and T_p = 3.5 (*triangles*), 3.7 (*circles*) and 3.9 GeV (*squares*) [14]. The *open circles* show the data taken at 2.5° and T_p = 2.1 GeV [12] and the *open squares* the pion cross sections measured at 10.7° and T_p = 5.5 GeV [15]. The *lines* show the fit using Eq. (3) to the data (see text), the star is the extracted cross section for the kinematical conditions of the present work

4 Extraction of absolute cross sections

In order to normalize the production cross sections we use the scaling behavior of $pA \to \pi X$ reactions [9, 10, 11]. In high-energy nucleon-nucleon interactions the pion yield does not depend on the incident energy but only on the Feynman scaling variable $x_F = p_l^*/p_{max}^{(\pi)}$, where p_l^* is the longitudinal momentum in the pN center-of-momentum (CM) system and

$$p_{max}^{(\pi)} = \left\{[s - (2m_N + m_\pi)^2][s - (2m_N - m_\pi)^2]/4s\right\}^{1/2} \quad (2)$$

with $s = 2m_N(2m_N + T_p)$ and m_N, m_π being the nucleon and pion mass, respectively. Papp et al. [12] and Moeller et al. [13] found that the scaling behaviour of pion production persists for proton-nucleus collisions down to an incident energy of 1 GeV.

In Fig. 6 the available published data on the invariant cross section of π^+ production in pBe collisions at proton energies from 2.1 to 5.5 GeV are shown as function of x_F. The solid line shows the best fit to the plotted experimental data in the form

$$E\,\frac{d^3\sigma}{d^3p} = a(1 - x_F)^b \quad (3)$$

with parameters a = (394±2) mb GeV^{-2} c^3 sr^{-1} and b = 4.0± 0.2. The dashed line represents Function (3) with a slope b = 3 predicted by Schmidt and Blankenbecler [16] and Landau and Gyulassy [17] with the hard scattering model employing the structure function of the nucleus and elementary $NN \to NN\pi$ processes.

The pions detected in the present measurement correspond to a value of x_F = 0.15. Nagamiya et al. [18, 19] showed that low-energy pions ($x_F < 0.2$) have an almost isotropic angular distribution. Therefore, the cross section for pions produced under emission angles of $\vartheta \approx 17°$ can be calculated using the data from [12, 14, 15] which were obtained at smaller emission angles. Normalizing our point with Function (3) we obtain for T_p = 2.9 GeV, ϑ = 17°, p_π = 0.545 GeV/c:

$$E\,\frac{d^3\sigma}{d^3p}(p\text{Be} \to \pi^+X) = 200 \pm 41 \pm 3 \text{ mb GeV}^{-2}\text{ c}^3\text{ sr}^{-1}, \quad (4)$$

shown in Fig. 6 by the star. The first error is due to the average uncertainty of the absolute normalization of the data from [12, 14, 15] which is not shown in Fig. 6. The second error is caused by the fitting procedure.

From the measured ratios (1) we then obtain the following cross section for protons

$$E\,\frac{d^3\sigma}{d^3p}(p\text{Be} \to pX) = 141 \pm 31 \text{ mb GeV}^{-2}\text{ c}^3\text{ sr}^{-1}, \quad (5)$$

and for K^+ mesons

$$E\,\frac{d^3\sigma}{d^3p}(p\text{Be} \to K^+X) = 3.1 \pm 1.2 \text{ mb GeV}^{-2}\text{ c}^3\text{ sr}^{-1}. \quad (6)$$

Figure 7 shows the invariant cross section for proton production in pBe collisions at energies from 3.5 to 6.6 GeV as a function of x_F calculated with

$$p_{max}^{(p)} = \left\{s/4 - m_N^2\right\}^{1/2}. \quad (7)$$

The line shows a fit to the data in the form

$$E\,\frac{d^3\sigma}{d^3p} = a\exp(bx_F) + cx_F + d. \quad (8)$$

The first term in (8) describes the well known exponential behaviour of the inclusive nucleon-production cross section in the target-fragmentation region [21]. The two last terms reflect the linear dependence of the invariant cross section in x_F predicted by Hwa [22] and Sibirtsev [23] in the projectile-fragmentation region $x_F > 0.1 \ldots 0.2$. The proton cross section deduced from the measured ratio and normalization of the pion cross section discussed above is shown in Fig. 7 by the star. Our point corresponds to $x_F = -0.44$, which is below the projectile-fragmentation region. The solid line in Fig. 7 shows Function (8) with parameters extracted from a fit not taking into account the cross section from this work. We obtain values of a = 0.43, b = −9.8, c = 20.4 and d = 43.1 with χ^2 = 0.9. There is good agreement between Function (8) and the data. A fit to the data including our point results in parameters a = 0.42, b = −9.9, c = 19.6 and d = 43.6 and χ^2 = 1.1. Taking into account that the data from [14, 20] shown in Fig. 7 were measured under quite different kinematical conditions we conclude that the superposition of the target- and projectile-fragmentation processes reasonably describes the transition region and that our cross section (5) is in agreement with previous measurements.

5 Analysis of K^+ production

Data on K^+ production in proton-nucleus collision at energies below or close to the free $pN \to K^+X$ threshold at T_p = 1.58 GeV are rather scarce. The total K^+-production cross sections in pA collisions at energies below 1 GeV were measured by

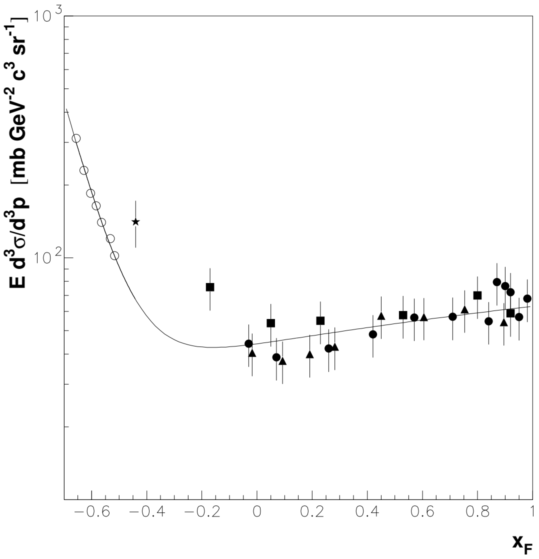

Fig. 7. Measured invariant cross sections for proton production. The *closed symbols* show the proton spectra measured at an emission angle of 3.5° and T_p = 3.5 (*triangles*), 3.7 (*circles*) and 3.9 GeV (*squares*) [14]. The *open circles* show the data obtained by Bayukov et al. [20] at 30° and T_p = 6.6 GeV. The *line* shows a fit to the data using Function (8) (see text), the *star* indicates the cross section from our experiment

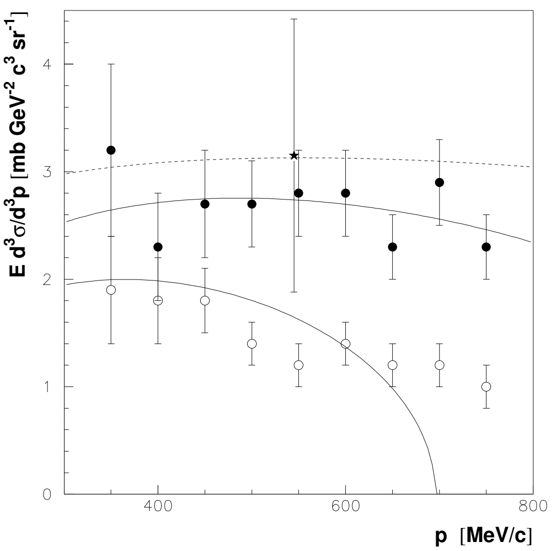

Fig. 8. Measured invariant cross sections for kaon production. The spectra were measured in p(NaF) collisions at T_p = 2.1 GeV and emission angles of 15° (•) and 35° (○) [25]. The *star* indicates the cross section from our experiment. The solid *lines* show Eq. (9) fitted to the data [25] (see text) and the dashed line the application of Eq. (9) to our data point

Abrosimov et al. [24] at the Petersburg Nuclear Physics Institute. Inclusive K^+ production in p(NaF) and pPb collisions at 2.1 GeV was studied at Bevalac [25]. The inclusive K^+ production has been studied in pC and pPb collisions at energies T_p = 1.2, 1.5, 2.5 GeV in a SATURNE/GSI experiment [26] and at energies from 1.65 to 2.9 GeV at ITEP, Moscow [27] for various target nuclei. The study of subthreshold K^+ production in pA collisions with correlation measurements is under preparation at COSY-Jülich [3]. It is also planned to study the K^+ production at proton energies down to 800 MeV at CELSIUS [28]. In Fig. 8 we show the K^+ spectra measured in p(NaF) collisions at T_p = 2.1 GeV and emission angles of 15° and 35° [25]. Our result for pBe collisions at 2.9 GeV and an emission angle of 17° is shown by the star.

The theoretical predictions for K^+ production in pA collisions were mostly made for total production cross sections. Thus for comparison with theories we calculate these total cross sections from the measured differential ones. We integrate the data shown in Fig. 8 assuming a phase-space dependence of kaon production. We use the following expression [29]:

$$E\,\frac{\mathrm{d}^3\sigma}{\mathrm{d}^3p}(pA \to K^+X) = \frac{\pi}{4}\cdot\frac{\sigma_{\mathrm{tot}}(pA \to K^+X)}{\Phi} \cdot\frac{\lambda(s_{\Lambda p}, m_\Lambda^2, m_p^2)}{s_{\Lambda p}} \qquad (9)$$

with m_Λ and m_p being the Λ-hyperon and proton mass and $s_{\Lambda p}$ the minimal residual mass satisfying baryon number and strangeness conservation:

$$s_{\Lambda p} = s - 2(T_p + 2m_p)E_K + 2p_p p_K \cos(\theta_K) + m_K^2\ . \qquad (10)$$

E_K, p_K, m_K and θ_K are the total energy, momentum, mass and the emission angle of the detected K^+ meson, respectively, and T_p, p_p the kinetic energy and momentum of the incident proton. The squared invariant mass s of the colliding nucleons is defined above and λ is the function

$$\lambda^2(x, y, z) = [x - (\sqrt{y} + \sqrt{z})^2][x - (\sqrt{y} - \sqrt{z})^2]\ . \qquad (11)$$

In (9) Φ is the phase-space volume

$$\Phi = \left(\frac{\pi}{2}\right)^2 \int_{s_{\min}}^{s_{\max}} \frac{\lambda(s_{\Lambda p}, m_\Lambda^2, m_p^2)}{s_{\Lambda p}} \cdot \frac{\lambda(s, s_{\Lambda p}, m_K^2)}{s} \mathrm{d}s_{\Lambda p} \qquad (12)$$

and $s_{\min} = (m_p + m_\Lambda)^2$, $s_{\max} = (\sqrt{s} - m_K)^2$.

In Fig. 8 the lines show our fit with (9) and one free parameter which is the total K^+-production cross section in pA collisions. The values of $\sigma_{\mathrm{tot}}(pA \to K^+X)$ obtained by fitting the data from [25, 26] and calculated with our point are shown in Table 4. We also present results from [25, 26] assuming an isotropic and exponential behavior of the kaon spectra in the CM system of the colliding nucleons, i.e.

$$\frac{\mathrm{d}^3\sigma}{\mathrm{d}^3p} = C\exp(-T^*/T_0)\ , \qquad (13)$$

where T^* is the kinetic energy of the K^+ meson in the CM system and the parameters C and T_0 were extracted from an analysis of the experimental data [25, 26]. Note that results from [25, 26] are around two times larger than our estimate. Approach (13) could not be applied to our data point since for a fit of the two parameters C and T_0 at least two points would be required.

6 Analysis of the A dependence of K^+ production

It has been widely discussed [1, 2, 32] that the strong dependence of the total K^+-production cross section on the target mass

Table 4. Values for the total K^+-production cross sections and the slope parameter α in (15) extracted from the data in [25, 26] and the present work. The values for $\sigma(pp)$ were taken from [30, 31]. The calculated pA cross sections using (13) were taken from [25, 26], whereas the cross sections from approach (9) were calculated by us from the measured double differential cross sections

			$\sigma_{\text{tot}}(pA)$ [mb]		α		
T_p [GeV]	Target	$\sigma(pp)$ [μb]	(9)	(13)	(9)	(13)	ROC
2.1	NaF	22	0.85 ± 0.10	1.8 ± 0.6	1.20 ± 0.04	1.45 ± 0.11	1.03 ± 0.07
2.1	Pb	22	5 ± 1	11 ± 4	1.02 ± 0.04	1.16 ± 0.07	0.75 ± 0.03
2.5	C	71	0.39 ± 0.05	0.75 ± 0.08	0.69 ± 0.05	0.95 ± 0.05	0.97 ± 0.05
2.9	Be	140	3.7 ± 1.5	–	1.48 ± 0.19	–	0.79 ± 0.06

$$\sigma_{\text{tot}}(pA \to K^+X) \propto A^\alpha \tag{14}$$

with the slope α being equal to $1.2 \ldots 1.3$ indicates a dominant contribution from the two-step reaction mechanism $pN_1 \to \pi X$, $\pi N_2 \to K^+X$. Moreover, the experimental study of subthreshold K^+ production [24] confirmed the theoretical prediction. The direct production $pN \to K^+X$ is assumed to be described by (14) with $\alpha \simeq 0.7$, see below.

Theoretical calculations made by Cassing et al. [1] and Sibirtsev and Büscher [2] demonstrate that the two-step reaction mechanism dominantly contributes to K^+ production at energies $T_p < 1.5$ GeV. At energies above 2 GeV the kaons are expected to be produced mainly via the direct reaction mechanism which is also confirmed by an analysis of experimental data on differential cross sections obtained at $T_p > 10$ GeV [33].

In order to calculate the slope parameter α from the total K^+-production cross sections we use the standard formula

$$\sigma_{\text{tot}}(pA \to K^+X) = \sigma(pp \to K^+X) \cdot A^\alpha \; . \tag{15}$$

With the elementary cross sections from [30, 31] and the experimental values from [25, 26] and this work we obtain values for α between 0.69 and 1.48 which are presented in Table 4. Note that our result for α obtained with (9) for T_p = 2.5 GeV and a C target is substantially smaller than all other slopes.

Following the folding model [1, 2] the A dependence of K^+ production in direct processes is determined by the effective number of target nucleons participating in the interaction [34]

$$N_{\text{eff}} = \frac{1}{\sigma} \int [1 - \exp(-\sigma T(\mathbf{b}))] \mathrm{d}\mathbf{b} \tag{16}$$

where σ is the total pp cross section. The profile function

$$T(\mathbf{b}) = \int \rho_A(\mathbf{b}, z) \mathrm{d}z \tag{17}$$

was calculated with a harmonic oscillator density for light nuclei [34] and the Woods-Saxon density for $A > 16$ [35]. Using these formulas we obtain N_{eff} = 5.2, 6.2, 10.1, 49.8 for Be, C, NaF and Pb target nuclei. A fit of N_{eff} with a function A^α results in an average slope $\alpha = 0.74 \pm 0.01$. Obviously, this result strongly contradicts our estimates from Table 4 obtained from the experimental data except for our value calculated with (9) for the C target.

In the table we also show the results of calculations using the Rossendorf-Collision (ROC) Model [36] which takes into account K^+ production in multi-nucleon collisions of the incident proton. The ROC model predicts an A dependence closer to the experimental results which may indicate contributions from multi-step processes even at projectile energies above 2 GeV.

7 Summary

We have measured K^+, π^+ and p production in pBe collisions at T_p = 2.9 GeV, ejectile momenta p = 545 MeV/c and emission angles $\vartheta = 17°$. The cross sections were normalized with available data on π^+ production in pBe collisions making use of the scaling behaviour of the cross sections on the Feynman variable x_{F}. We found that our result for the proton production cross section is in good agreement with published data.

In order to compare the experimental result on K^+ production with theoretical predictions on the total production cross section we integrated our data as well as the data from [25] at T_p = 2.1 GeV assuming a phase-space distribution. The integrated K^+ cross section from pC collisions at 2.5 GeV recently obtained in an SATURNE/GSI experiment [26] is also included in our analysis. The A dependence of the total K^+-production cross section can be described by a function A^α. In the energy range $T_p = 2.1 \ldots 2.9$ GeV we obtain for the slope α values which are in the range $0.69 \ldots 1.48$ for four different target nuclei (Be, C, NaF, Pb).

Theoretical calculations with the folding model based on the assumption of a dominant contribution from the direct reaction mechanism to K^+ production in pA collisions predict a slope $\alpha = 0.74 \pm 0.01$ if one averages over the target nuclei used in the measurements. This value is in strong disagreement with most of the experimental values.

The Rossendorf-Collision Model which also takes into account K^+ production in multi-nucleon collisions predicts a slope $\alpha = 0.79 \ldots 1.03$ which is closer to the experimental results.

We summarize that our study may indicate the importance of multi-nucleon mechanisms for K^+ production in pA reactions at energies above the nucleon-nucleon threshold. However, more definite conclusions need further experimental studies, in particular on the A dependences of the total production cross sections.

Acknowledgement. During the data analysis we were informed about the first experimental results on K^+ production obtained in the SATURNE/GSI experiment. We thank M. Debowski, E. Grosse and P. Senger for sharing the data with us prior to publication and for useful discussions.

References

1. Cassing, W., Batko, G., Mosel, U., Niita, K., Schult, O., Wolf, G.: Phys. Lett. B **238**, 25 (1990)

2. Sibirtsev, A.A., Büscher, M.: Z. Phys. A **347**, 191 (1994)
3. Borgs, W.,Büscher, M., Gotta, D. et al.: COSY Proposal 18 Jülich 1990
4. Büscher, M., Sistemich, K., Abaev, V. et al.: Physica Scripta **48** 50 (1993)
5. Barmin, V.V., Golubchikov, V.M., Gorochov, A.I. et al.: Preprint ITEP-99, Moscow 1977
6. CAMDA: A CAMAC-PC Data Acquisition System, Physikalische Nachweisgeräte Dr. Herbert Stelzer, Zimmernerstr. 9, 64409 Messel
7. Sheinkman, V.A.: private communication
8. Theiss, D.: Ph.D. Thesis, Universität Bonn (1992)
9. Taylor, F.E., Carey, D.C., Johnson, J.R., Kammerud, R., Ritchie, D.J., Roberts, A., Sauer, J.R., Shafer, R., Theriot, D., Walker, J.K.: Phys. Rev. D **14**, 1217 (1976)
10. Johnson, J.R., Kammerud, R., Ohsugi, T., Ritchie, D.J., Shafer, R., Theriot, D., Walker, J.K., Taylor, F.E.: Phys. Rev. D **17**, 1292 (1978)
11. Barton, D.S., Brandenburg, G.W., Busza, W., Dobrowolski, T., Friedman, J.I., Halliwell, C., Kendall, H.W., Lyons, T., Nelson, B., Rosenson, L., Verdier, R., Chiaradia, M.T., DeMarzo, C., Favuzzi, C., Germinario, G., Guerriero, L., LaVopa, P., Maggi, G., Posa, F., Selvaggi, G., Spinelli, P., Waldner, F., Cutts, D., Dulude, R.S., Hughlock, B.W., Lanou, R.E., Massimo, J.T., Brenner, A.E., Carey, D.C., Elias, J.E., Garbincus, P.H., Polychronkas, V.A., Nassalski, J., Siemiarczuk, T.: Phys. Rev. D **27**, 2580 (1983)
12. Papp, J., Jaros, J., Schroeder, J., Staples, J., Steiner, H., Wagner, A., Wiss, J.: Phys. Rev. Lett. **34**, 601 (1975)
13. Moeller, E., Anderson, L., Brückner, W., Nagamiya, S.,Nissen-Meyer, S.,Schroeder, L.,Shapiro, G., Steiner, H.: Phys. Rev. C **28**, 1246 (1983)
14. Vorontsov, I.A., Safronov, G.A.,Sibirtsev, A.A., Smirnov, G.N., Trebuchovsky, Y.V.: Preprint ITEP-144, Moscow 1984
15. Lepikhin, Y., Pasko, S., Smirnitsky, A., Sheinkman, V.: Sov. J. Nucl. Phys., *to be published*
16. Schmidt, A., Blankenbecler, R.: Phys. Rev. D **15**, 3321 (1977)
17. Landau, R.H., Gyulassy, M.: Phys. Rev. C **19**, 149 (1979)
18. Nagamiya, S., Niessen-Meyer, S., Schroeder, L., Shapiro, G., Steiner, H.: Phys. Rev. C **28**, 1246 (1983)
19. Nagamiya, S., Lemaire, M.-C., Moeller, E., Schnetzer, S., Shapiro, G., Steiner, H., Tanihata, I.: Phys. Rev. C **24**, 971 (1981)
20. Bayukov, Y.D., Vlasov, A.V., Gavrilov, V.B., Goryainov, N.A., Grishuk, Y.G., Guchin, O.B., Degtyarenko, P.V., Kornienko, N.L., Kosov, M.V., Kuleshova, L.N., Leksin, G.A., Suchkov, D.A., Fedorov, V.B., Shvartsman, B.B., Shevchenko, S.V., Shuvalov, S.M., Yakovlev, R.M.: Preprint ITEP-5, Moscow 1985
21. Boyarinov, S.V., Evseev, I.I., Kiselev, Y.T., Leksin, G.A., Martemyanov, A.N., Mikhailov, K.R., Pozdnyakov, S.A., Terekhov, Y.V., Ushakov, V.I., Sheinkman, V.A.: Phys. At. Nucl. **57**, 1379 (1994)
22. Hwa, R.C.: Phys. Rev. Lett. **52**, 492 (1984)
23. Sibirtsev, A.A.: Preprint ITEP-47 Moscow 1993
24. Abrosimov, N.K., Volchenkov, V.A., Gridnev, A.B., Eliseev, V.A., Ivanov, E.M., Koptev, V.P., Kruglov, S.P., Malov, Y.A., Kikirtych' yants, S.M., Ryabov, G.A., Shcherbakov, G.V.: JETP Lett. **43**, 271 (1986)
25. Schnetzer, S., Lombard, R.M., Lemaire, M.-C., Moeller, E., Nagamiya, S., Shapiro, G., Steiner, H., Tanihata, I.: Phys. Rev. C **40**, 640 (1989)
26. Debowski, M.: Ph.D. Thesis, Cracow 1995
27. Chumakov, M., Kiselev, Y., Martemyanov, A., Mikhailov, K., Sheinkman, V.: ITEP Proposal, Moscow 1993
28. Palmeri, A., Badala, A., Barbera, R., Bonasera, A., Ekström, C., Ericsson, G., Höistad, B., Johansson, R., Johansson, T, Pappalardo, G.S., Riggi, F., Russo, A.C., Traneus, E., Turrisi, R., Westerberg, L.: CELSIUS Proposal, Uppsala 1994
29. Efremov S.V., Kazarnovsky, M.V., Paryev, E.Y.,: Z. Phys. A **344**, 181 (1992)
30. Flaminio, V., Moorhead, W.G., Morrison, D.R.O., Rivoire, N.: Compilation of cross sections, CERN-HERA 84-01 (1984) Geneva
31. Sibirtsev, A.A., Müller, H., Schneidereit, Ch.: sub. to. Phys. Lett.
32. Koptev, V.P., Mikirtych' yants, S.M., Nesterov, N.A., Tarasov, N.A., Shcherbakov, G.V., Abrosimov, I.K., Volchenkov, V.A., Gridnev, A.B., Eliseev, V.A., Ivanov, E.M., Kruglov, S.P., Malov, Y.A., Ryabov, G.A.: JETP **67**, 2177 (1988)
33. Sibirtsev A.A.: Sov. J. Nucl. Phys. **55**, 145 (1992)
34. Glauber, R.J., Mathiae, J.: Nucl. Phys. B **21**, 135 (1970)
35. Knoll, J., Randrup, J.: Nucl. Phys. A **342**, 445 (1979)
36. Müller, H.: Z. Phys. A **339**, 409 (1991)

This article was processed by the author using the LaTeX style file *pljour2* from Springer-Verlag.